# Evaluation of chemistry models on methane/air edge flame simulation

Bastien Duboc, Guillaume Ribert, Pascale Domingo

▶ **To cite this version:**

Bastien Duboc, Guillaume Ribert, Pascale Domingo. Evaluation of chemistry models on methane/air edge flame simulation. Proceedings of the Combustion Institute, 2019, 37 (2), pp.1691-1698. 10.1016/j.proci.2018.05.053 . hal-02007802

**HAL Id: hal-02007802**

**https://normandie-univ.hal.science/hal-02007802**

Submitted on 4 Dec 2020

**HAL** is a multi-disciplinary open access archive for the deposit and dissemination of scientific research documents, whether they are published or not. The documents may come from teaching and research institutions in France or abroad, or from public or private research centers.

L'archive ouverte pluridisciplinaire **HAL**, est destinée au dépôt et à la diffusion de documents scientifiques de niveau recherche, publiés ou non, émanant des établissements d'enseignement et de recherche français ou étrangers, des laboratoires publics ou privés.

# Evaluation of chemistry models on methane/air edge flame simulation

Bastien Duboc[a], Guillaume Ribert[a,*], Pascale Domingo[a]

[a]*CORIA - CNRS, Normandy Université, INSA de Rouen Normandie*
*76000 Rouen, France*

**Abstract**

The integration of chemistry into a numerical fully compressible solver is carried out in this study using three models: detailed chemistry, fully tabulated chemistry (CTC) and a model coupling both approaches called HTTC, for hybrid transported-tabulated chemistry. With HTTC major species are transported while most minor species are tabulated. As minor species are no longer transported with the flow, the time step is close to the values usually encountered for non-reactive flows, far beyond what is found in detailed chemistry. The performance of HTTC for reproducing the dynamics of a methane/air edge flame featuring a very strong mixture fraction gradient is also investigated. The results agree favorably with the reference case simulated with detailed chemistry unlike the CTC model which is unable to predict the topology of the flame. Finally, the shape of the flame, the flame speed and the flame stabilization height are reasonably well captured with HTTC with a calculation cost divided by about 5 compared to the reference case.

*Keywords:* Hybrid chemistry, Compressible solver, Edge flame, DNS

- **Corresponding author**:
  - Last name: Ribert
  - First name: Guillaume
  - Mailing address:
    CORIA - CNRS and INSA de Rouen,
    Avenue de l'Université, 76800 Saint-Etienne-du-Rouvray, France
  - Phone number: +33(0)2 32 95 97 92
  - Email: guillaume.ribert@coria.fr

- **Colloquium 4**: Laminar flames
- **Abstract**: 160 words
- **Article, total length**: $6000 = 6 \times 900 + 2.2 \times$ 270 mm with the two-column method (LaTeX)
- **Color figures**: not applicable

*Corresponding author
*Email address:* guillaume.ribert@coria.fr
(Guillaume Ribert)

## 1. Introduction

Introducing fully detailed schemes in numerical simulations for combustion is still a scientific challenge. In practical situations, it cannot be achieved because the number of species and reactions are way too large [1]. Instead of detailed chemistry (acronym FTC), reduced kinetics or tabulated thermochemistry (CTC) may be used [2]. The first strategy may lead to inaccuracy if the reduced scheme is not optimized [3] because minor species and radicals are missing. If done carefully, the resulting reduced schemes compare well with the original detailed mechanism on the dedicated range of validity. The second approach is based on the tabulation of chemical responses of canonical combustion problems such as one-dimensional laminar premixed flames [4, 5]. These structures are often projected into a progress variable and mixture fraction space to build a look-up table. Thus, only these two variables need to be transported with the flow, dramatically reducing the computational cost. However, such tables are cumbersome to create, lack of flexibility and may lead to very large database not suited to the context of high-performance computing. Hence, table downsizing methods have been discussed in the literature, using the self-similarity behavior of the radical species in laminar flamelets [6, 7] or ignition phenomena [8, 9]. This property has been further exploited by Ribert *et al.* [10] to develop a strategy combining the detailed-chemistry solving for the main species with the tabulation of the intermediate species, called Hybrid Transported-Tabulated Chemistry (HTTC).
CTC and HTTC models are presently evaluated on the challenging configuration of a methane/air edge flame featuring a large gradient of mixture fraction, and compared with results coming from detailed chemistry. In such configurations, the reactants are partially premixed before burning, and an edge flame is present consisting of a premixed flame front divided into a lean and a rich zone, followed by a trailing diffusion flame, that burns the excess of the reactants downstream [11]. The whole range of equivalence ratio ($\phi$) from pure fuel to pure oxidizer is then present making the simulation challenging for any combustion models.

## 2. Chemistry modeling and numerical solver

Dealing with a chemical system composed of $N_S$ species ($S = \{1, \cdots, N_S\}$) reacting through $N_R$ reactions ($R = \{1, \cdots, N_R\}$) requires to write one transport equation for each species $k \in S$ when using a FTC solver:

$$\frac{\partial \rho Y_k}{\partial t} + \frac{\partial}{\partial x_i}\left(\rho[u_i + V_{k,i} + V_i^c]Y_k\right) = \dot{\omega}_k, \quad k \in S. \quad (1)$$

$x_i$, $t$ and $u_i$ are the spatial coordinates, time and $i$th-velocity components, respectively. $\rho$ is the density defined as $\rho = \sum_S \rho_k$, with $\rho_k = \rho Y_k$. $Y_k$ is the mass fraction of species $k$ with $\sum_S Y_k = 1$, $V_{k,i}$ is the diffusion velocity of species $k$ computed with the Hirschfelder and Curtiss approximation [12], $V_i^c$ is the correction velocity to ensure the mass conservation and $\dot{\omega}_k$ is the chemical source term of species $k$ with $\sum_S \dot{\omega}_k = 0$.
At the extreme opposite, CTC methods [13, 14] assume that chemical evolutions in the composition space are parameterized by a reduced set of $N_t$ variables such as the progress variable, $Y_c$, the mixture fraction, $Z$, enthalpy, etc. that are transported with the flow. The $N_S$ transport equations used with the FTC solver are replaced in CTC by $N_t$ ($\ll N_S$) equations plus a look-up table containing all the expected flame structures. The balance equation for $Y_c$ is formally written:

$$\frac{\partial \rho Y_c}{\partial t} + \frac{\partial}{\partial x_i}\left(\rho u_i Y_c\right) = \frac{\partial}{\partial x_i}\left(\rho D_{Y_c} \frac{\partial Y_c}{\partial x_i}\right) + \dot{\omega}_c, \quad (2)$$

with $Y_c = \sum_{k\in S} \alpha_k Y_k = Y_{CO_2} + Y_{CO}$ in this study, and $\dot{\omega}_c = \dot{\omega}_{CO_2} + \dot{\omega}_{CO}$. The diffusion coefficient $D_{Y_c}$ is computed in the present work with the species diffusion coefficients, $D_k$, as

$$D_{Y_c} = \sum_{k\in S} \alpha_k \left|\frac{\partial Y_k}{\partial Y_c}\right| D_k = \left|\frac{\partial Y_{CO_2}}{\partial Y_c}\right| D_{CO_2} + \left|\frac{\partial Y_{CO}}{\partial Y_c}\right| D_{CO}, \quad (3)$$

to ensure a proper flame speed. $\dot{\omega}_c$ and $D_{Y_c}$ are part of the look-up table and depend on $N_t$ variables. $Z$ is transported with a unity Lewis number assumption as in [15].
With HTTC [10], the whole kinetic scheme is kept unaltered meaning that the knowledge of the $N_S$ species mass fractions is required, but the set of chemical species is splitted in a set of major ($M = \{1, \cdots, N_M\}$) and minor ($m = \{1, \cdots, N_m\}$) species: $N_S = N_M + N_m$. Major species are transported with the flow and the mass fractions of minor species come from generic laws observed in the simulations of canonical problems. For minor species, the self-similar flame tabulation (S2FT) technique [6, 7, 8] is presently exploited. This reduced look-up table is accessible by $Y_c$ and $Z$ (or $\phi$) [16]. Eq. (1) is then replaced by

$$\frac{\partial \rho Y_k}{\partial t} + \frac{\partial}{\partial x_i}\left(\rho[u_i + V_{k,i} + V_i^c]Y_k\right) = \dot{\omega}_k, \quad k \in M \quad (4)$$

plus a look-up table (S2FT),

$$Y_k = f(Y_c, Z), \quad k \in m. \tag{5}$$

In Eq. (4), the computation of $\dot{\omega}_k$ requires the evaluation of the rate-of-progress of all elementary reactions of the kinetic scheme. For any species $k \in m$, $Y_k$ is directly evaluated with Eq. (5) and not through a transport equation anymore. Finally, $V_i^c$ in Eq. (4) is evaluated based on transported species only ($k \in M$): $V_i^c = -\left(\sum_M V_{k,i} Y_k\right) \Big/ \sum_M Y_k$. This strategy has been successfully applied to the computation of 1D laminar methane/air premixed flames with the REGATH numerical code [17, 18] in which transport equations are solved for a constant pressure with a Newton algorithm. The three solvers FTC, CTC and HTTC are presently considered within the finite volume solver DNS/LES SiTCom-B [14, 19, 20] that explicitly solves the unsteady fully compressible and reactive Navier-Stokes equations on cartesian meshes. From a numerical point of view, solving Eqs. (4) in addition to the momentum and energy equations in SiTCom-B requires to evaluate the density at each time step based on the contribution of major and minor species. However, the mass fractions of minor species are only accessible through the knowledge of the table parameters $(Y_c, Z)$ which are unknown at each time step $n$. As a consequence,

$$\rho^n = \sum_M \rho_k^n + \sum_m \rho_k^{n-1} \tag{6}$$

with $(\sum_m \rho_k)^{n-1} \ll (\sum_M \rho_k)^n$ for all $n$ [10]. The error on $\rho^n$ is estimated to be very small since the variations of the quantities from two consecutive time steps should be small with a compressible code. Once the density is known, the mass fraction of major species can be determined by $Y_k^n = \rho_k^n/\rho^n, k \in M$ as well as the table parameters: $Y_c^n$ and $Z^n$. Minor species are given by Eq. (5) and any $\dot{\omega}_k, k \in M$ can be properly computed.

The implementation of the three solvers into SiTCom-B has been validated by simulating a stoichiometric 1D laminar premixed methane/air flame with a variable Lewis number and without $NO_x$ chemistry. The kinetic scheme of Lindstedt and co-workers is used [21] ($N_S = 29$: H, OH, O, $HO_2$, $H_2$, $H_2O$, $O_2$, CO, $CO_2$, $N_2$, CH, HCO, $CH_2$(S), $CH_2$, $CH_2O$, $CH_3$, $CH_3O$, $CH_2OH$, $CH_4$, $C_2H$, HCCO, $C_2H_2$, $CH_2CO$, $C_2H_3$, $C_2H_4$, $C_2H_5$, $C_2H_6$, C, and $C_2$; $N_R = 141$) as in [10]. A comparison with the solution given by REGATH is provided in Fig. 1. With HTTC, the following criterion is used to split the $N_S$ species in major and minor species: the reactants and products having a non-zero mass fraction,

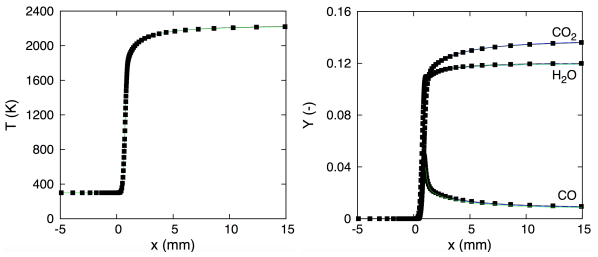


(a) Temperature (b) Major species

Figure 1: One-dimensional atmospheric $CH_4$/air flame at $\phi = 1$. Mesh resolution in the flame front: $\Delta x = 20$ µm. Squares: REGATH. Lines: SiTCom-B (black solid: FTC, blue solid: HTTC, green solid: CTC).

i.e. $Y_k > \epsilon = 1 \times 10^{-8}$ for all $\phi$ used to compute the look-up table, in the fresh and the burnt gases, are transported. Accordingly, for $\phi \in [0.6, 1.4], N_M = 13$ ($O_2$, $N_2$, $CO_2$, CO, $H_2O$, $H_2$, OH, O, H, $HO_2$, HCO, $CH_2O$, $CH_4$) and $N_m = N_S - N_M = 16$. In Fig. 1 a very good agreement is found between the three solvers used. With SiTCom-B, a pressure jump across the flame front, $\Delta P_{\text{Num}} = -1.01$ Pa, is found in agreement with theory: $\Delta P_{\text{Th}} = \rho_u S_L^2 (1 - \rho_u/\rho_b) = -1.03$ Pa with the flame speed $S_L = 37.42$ cm/s and the unburnt and burnt density set to $\rho_u = 1.130$ kg/m$^3$ and $\rho_b = 0.1498$ kg/m$^3$, respectively. To ensure a stable temporal integration, the maximum time step used by the three solvers are $9.9 \times 10^{-9}$ s for FTC and $3.1 \times 10^{-8}$ s for HTTC and CTC. For the last two, the computational cost is reduced by a factor 3 thanks to the increase of the global time step, the cost per time step being roughly 10% less with HTTC than with FTC using Lindstedt's mechanism for methane combustion. Indeed, tabulating the minor species with HTTC allows for a strong increase of the chemical time step, which is the bottleneck of fully explicit compressible FTC solvers. In the present simulation, the data mining for CTC and HTTC has no impact on the CPU time.

## 3. Simulation setup and HTTC generalization

### *3.1. Simulation setup*

The simulation setup is a pure methane slot injector surrounded by a co-flow of air, so that a steady laminar edge flame can stabilize above the burner. The width of the slot is $D_f = 2$ mm, and the thickness of the injector wall is 0.5 mm. The simulated area along with the boundary conditions is given in Fig. 2. It consists in a two-dimensional domain, 15 millimeters wide

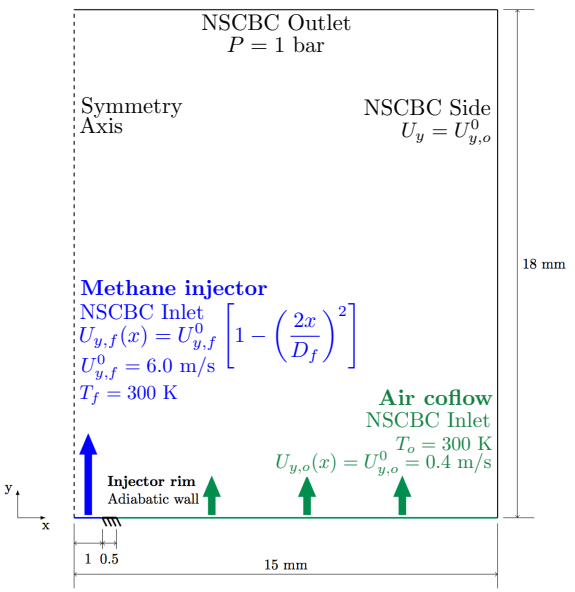


Figure 2: Dimensions and boundary conditions of the simulation domain.

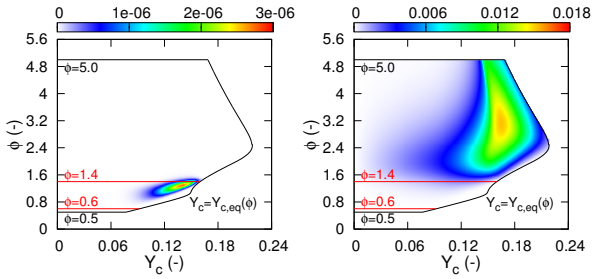


Figure 3: Species mass fraction of radical species C (left) and $C_2H_2$ (right) in the original 1D methane flame database ($\phi \in [0.5, 5.0]$), as a function of $Y_c$ and $\phi$.

and 18 millimeters high, beginning at the injector outlet, the goal being to simulate the tip of the edge flame. The domain is uniformly meshed with 50 micrometer cells. Simulations are performed with the three solvers: FTC, CTC and HTTC. The detailed kinetic mechanism of Lindstedt [21] without NOx has been used as in [10]. For FTC and HTTC, species are transported with variable Lewis numbers. The tabulated species mass fractions are stored using uniform $Y_c$ and $Z$ meshes, with small discretization step $\Delta Y_c = 5{\times}10^{-4}$ and $\Delta Z = 0.001$, to ensure that the parts of the table with strong derivative of the tabulated species mass fraction with respect to $Z$ and $Y_c$ are described with a sufficient accuracy. A change of table size would have a limited impact on CPU time because the code used to access the table has been carefully optimized. Unsteady simulations are run until a steady state of the laminar flow is reached, i.e. when the stabilisation height of the flame tip and the maximum temperature in the domain become constant. The flame tip (located at a height $y_0$) is defined as the intersection of the stoichiometric mixture fraction ($Z_{st}$) isoline and an isoline of a small value of the progress variable ($Y_c = 0.005$).

### *3.2. Generalization of HTTC*

The flame databases required in CTC and HTTC formulations have been initially generated for a range of equivalence ratio between the flammability limits of $CH_4$/air premixed flames, i.e. for $\phi \in [0.6, 1.4]$. For cases where chemical reactions take place on a wider range of $\phi$, such as in triple or edge flames, look-up tables need to be completed [15, 22, 23] or prolonged [14, 24]. The latter strategy is presently used for the CTC method. It consists of an extension of all the tabulated variables (temperature, transport coefficients, etc.) out of the flammability range by a linear interpolation between the fresh and equilibrium states. The chemistry is not extended ($\dot{\omega}_c = 0$) since the chemical activity or $S_L$ is low out of the flammability limits.

However, such a method cannot be directly transposed for HTTC. Indeed, the tabulated minor species mass fractions are zero both in the fresh gases and in the burnt gases, at equilibrium. Then, for equivalence ratios out of the flammability limits, their interpolated values would be 0. For many minor species this would lead to a gross error since they may take quite large values at the flammability limit. In figure 3, the mass fraction of C and $C_2H_2$ in methane/air flames, extracted from the 1D premixed database are plotted in a $(Y_c, \phi)$ space. It appears that both these minor species are not equal to zero at the rich boundary ($\phi = 1.4$). At the lean boundary ($\phi = 0.6$), some radical species such as $C_2H_5$, do not fade to zero either (not shown). The proposed extension method consists in generating additional flames out of the flammability limits, using the 1D flame solver REGATH. Even if it has been shown in experiments that premixed flames cannot propagate beyond these limits, REGATH is still able to provide data to extend the table. Accordingly, the range of $\phi$ has been augmented from $[0.6, 1.4]$ to $[0.5, 5]$ even if the results given by the 1D flame solver cannot strictly be considered as premixed propagating flames for very lean or very rich mixtures. Indeed for $\phi > 2.5$, the flame front propagates at velocities smaller than 1 cm/s and is very wide. The 10

meter-long domains used to generate the database are not even sufficient to reach equilibrium values for all minor species. The extended HTTC table is also displayed in Fig. 3. For most of the tabulated species, their mass fraction reaches zero for values of the progress variable smaller than the equilibrium value. Moreover, for $\phi > 2$, these species have a negligible mass fraction, whatever the value of $Y_c$, so the part of the flame database for high values of $\phi$ is not used. This is, for example, the case for C. Such an extension of the table will then be a satisfactory approach for such species. Nevertheless, a few radical species are still present at high equivalence ratios with a non-negligible mass fraction (e.g. $C_2H_2$). For these high values of $\phi$, they do not even reach equilibrium at the end of the computational domain, so a part of the table is missing for these species. Besides, their mass fractions at the rich equivalence ratio boundary of the table are still not zero. These species will then be transported instead of being tabulated. Consequently, when using the extended table, 7 species ($C_2H_2$, $C_2H_3$, $C_2H_4$, $C_2H_5$, $C_2H_6$, $CH_2CO$, $CH_3$) are added to the set $M$ of the transported species ($N_M = 20$). However, this additional cost does not affect the maximum time step used in simulations, the limiting species being still tabulated, and does not change the code efficiency.

## 4. Edge flame simulations

### *4.1. Flame structure with FTC*

The field of heat release rate (HRR) is displayed in Fig. 4(a). A lean and a rich premixed zone exist along with a trailing diffusion flame but the premixed wings are merged with the diffusion flame exhibiting a monobrachial structure, as in [11], because of the large values of $\nabla Z$ ($60\ \mathrm{m}^{-1} < \nabla Z < 120\ \mathrm{m}^{-1}$ on the isoline $Z_{st}$) and the low value of the radius of curvature of the flame, $R_c$, compared to the thermal flame thickness, $\delta_T$. A minimum value of $R_c = 0.5$ mm is found on the isoline HRR $= 0.05\ \mathrm{GW/m^3}$, significantly smaller than $\delta_T \approx 1$ mm. This is consistent with the observations made by Kim *et al.* [25], where the curvatures of edge-flames is found close to $R_c = 1$ mm in flows featuring gradients of mixture fraction around $50\ \mathrm{m}^{-1}$ on the isoline $Z_{st}$. The maximum of HRR is located nearby the stoichiometric line, at the triple point, where the three parts of the flame merge. The temperature of the flow increases along the stoichiometric line downstream of the premixed front (Fig. 4(b)) because of the presence of the diffusion trailing flame. The flame tip stabilizes

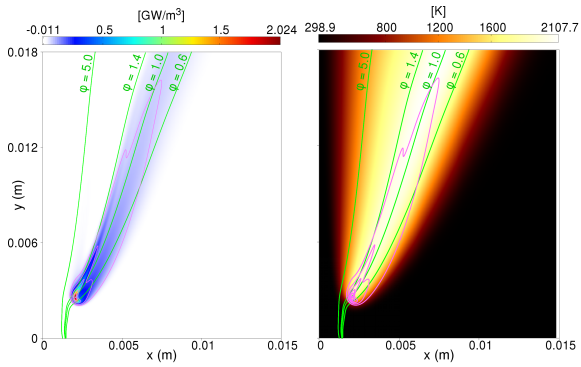


(a) Heat release rate (b) Temperature

Figure 4: Edge flame simulated with the FTC solver. In green: isolines of $Z$ corresponding to $\phi = 0.6$, 1.0, 1.4 and 5.0. In pink: isolines of heat release rate (0.05, 0.2, 0.5, 1.0, 1.5 and 2.0 $\mathrm{GW/m^3}$).

approximately 2 mm above the burner rim, at a radial location where the velocity of the flow is small enough to allow for the flame stabilization.

The contours of HRR plotted in Fig. 4(a) show that the premixed flame front is inclined with respect to the axial direction of the flow. Kim *et al.* [25] have attributed this phenomenon to the effect of the velocity gradient, which is usually strong in jet flames. As a consequence, the propagation velocity of the flame tip cannot be equal to the axial velocity of the flow at the triple point. Following [25], the propagation velocity is assumed to be equal to the velocity $U_n$ normal to the premixed front, which is presently calculated from the velocity vector $U$ at the flame tip: $U_n = U \cdot \nabla Y_c / |\nabla Y_c|$. $U_n = 0.209$ m/s while the 1D laminar flame speed is $S_L(\phi = 1) = 0.367$ m/s. This smaller propagation speed is due to the strong gradient of mixture fraction at the flame tip.

Finally, the reactive points of the simulated domain that contribute to the HRR (HRR $> 1\%$ of max (HRR)) are plotted in a $(Y_c, Z)$ space in Fig. 5. The flammability limits are here defined as the range of $\phi$ where reactive points are found (as in [26]). Even if this definition of the flammability range is different of what is used in experimental studies, it is clear that the limits are extended in the premixed zone, for $\phi$ ranging from 0.15 to 2.73. However, the reactive points that contribute to the diffusion flame are mainly found between $\phi = 0.6$ and $\phi = 1.4$, and for large values of $Y_c$, because they are located in the burnt gases downstream of the premixed flame front. The maximum of HRR is found in the premixed area of the flame, but HRR is still significant in the diffusion trailing flame. Finally, reactive points are found beyond the equilibrium line, which is

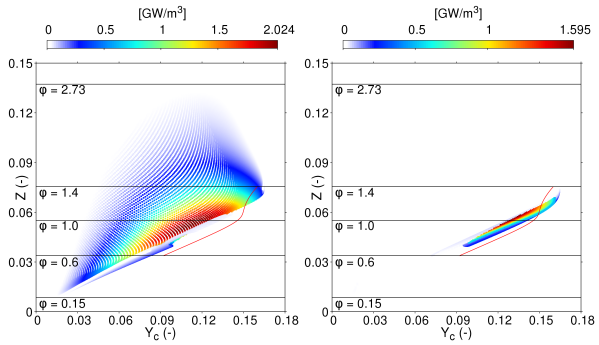


(a) Premixed flame (b) Diffusion flame

Figure 5: Scatter plot of HRR (only for HRR > 1% of max (HRR)) for FTC simulations. (a) premixed flame, |FI| = 1, (b) diffusion flame, |FI| = 0. The red line is the equilibrium extracted from the 1D database. FI: flame index [26].

extracted from the 1D premixed flame database. Such a phenomenon may be due to the presence of the diffusion tail, and to the diffusion of $Y_c$ from the rich side to the lean side of the flow.

### 4.2. Edge flame simulation with CTC and HTTC

*CTC simulation.* In figure 6(a), a stoichiometric isoline of mixture fraction ($Z_{st}$) and an isoline of progress variable, $Y_c = 0.005$, are plotted to visualize the shape and the stabilization height of the edge flames. The CTC

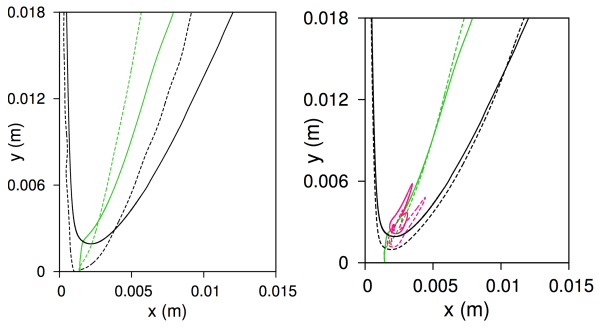


(a) CTC vs. FTC (b) HTTC vs. FTC

Figure 6: Comparison between CTC/HTTC and FTC simulations. Isolines of $Z_{st}$ (green) and $Y_c = 0.005$ (black) for FTC (solid lines) and CTC/HTTC (dashed lines). HRR in red.

method predicts that the flame is attached to the adiabatic burner wall contrary to what is observed with the FTC approach. Indeed, the whole modeling of the chemistry being constrained by the look-up table, and only accessible by the local values of $Z$ and $Y_c$, the impact of $\nabla Z$ is totally overlooked since it has not been taken into account in the generation of the table. As

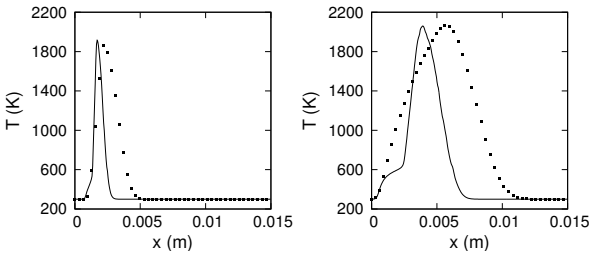


(a) $T$ at $y_0$ + 1 mm (b) $T$ at $y_0$ + 10 mm

Figure 7: Radial profiles of temperature at two heights above the flame tip ($y_0$), for FTC (symbols) and CTC (lines).

a consequence, the profiles of temperature taken at two heights above the flame tip differ from the reference case (FTC), even if the maximum values of the temperature are close (Fig. 7). Enlarging the range of $\phi$ as for the HTTC procedure has been tested without any further improvement on the propagation speed. To alleviate this issue inherent to tabulation methods, Nguyen *et al.* [27] proposed a multi-dimensional tabulation approach that takes the fluxes in the $Z$ direction into account during the generation of the manifold. However, a five dimensions look-up table is needed, complicating the CTC procedure and increasing its numerical cost.

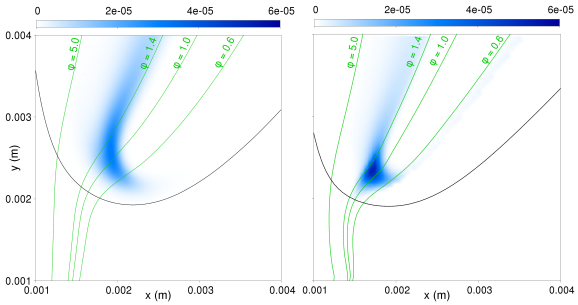


(a) FTC (b) HTTC

Figure 8: Mass fraction of $C_2H_5$ (zoom) computed $Z$ and $Y_c = Y_{CO} + Y_{CO_2}$. Green: isolines of $\phi$. Black: isoline of $Y_c = 0.005$.

*HTTC simulation.* In Fig. 6(b) the flame structure computed with HTTC is found very close to the reference flame (FTC). With HTTC, the flame stabilizes at $y_0 = 0.89$ mm, instead of 1.99 mm with FTC, because the propagation speed is slightly higher ($U_n = 0.215$ m/s) than with FTC ($U_n = 0.209$ m/s). A very good agreement with the reference temperature and mass fractions is obtained in Fig. 9 at three axial positions whatever the dominant combustion regime: premixing at

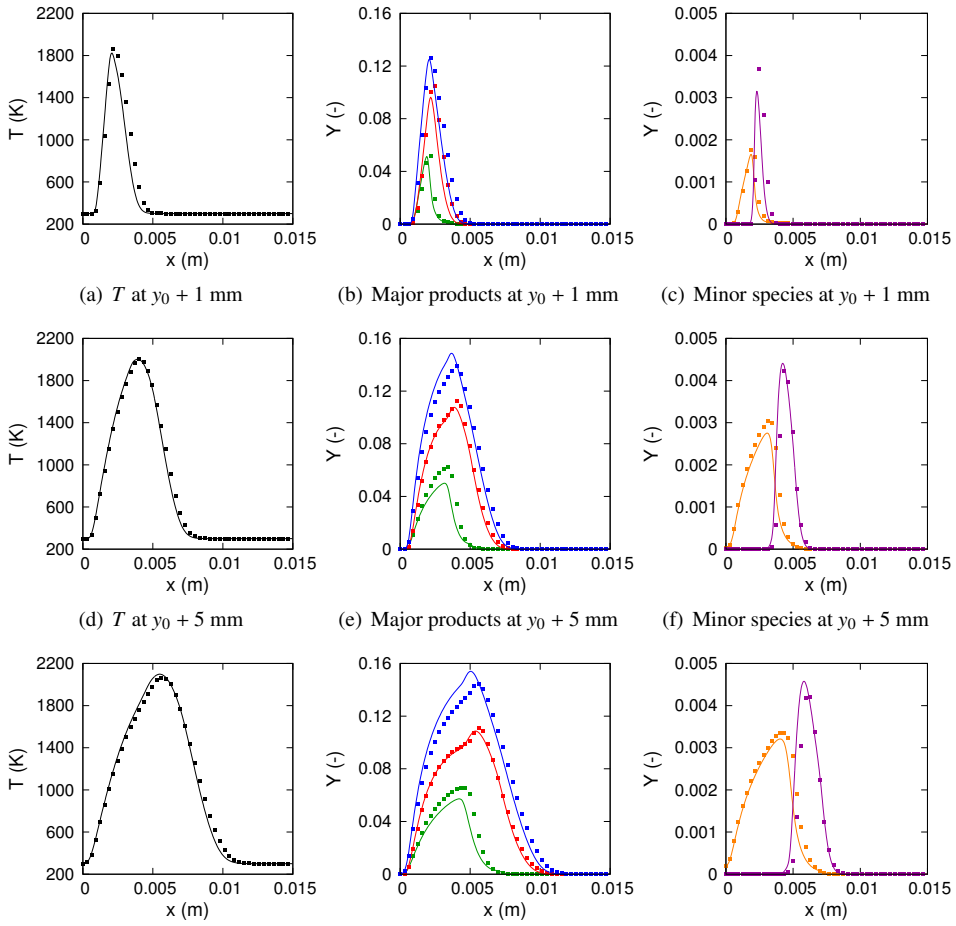


(a) $T$ at $y_0$ + 1 mm (b) Major products at $y_0$ + 1 mm (c) Minor species at $y_0$ + 1 mm

(d) $T$ at $y_0$ + 5 mm (e) Major products at $y_0$ + 5 mm (f) Minor species at $y_0$ + 5 mm

(g) $T$ at $y_0$ + 10 mm (h) Major products at $y_0$ + 10 mm (i) Minor species at $y_0$ + 10 mm

Figure 9: Radial profiles of temperature (black), major products (CO in green, $CO_2$ in red and $H_2O\times1.2$ in blue) and minor species (OH in purple and $H_2$ in orange) at different heights above the flame tip ($y_0$), for the FTC (symbols) and HTTC (lines) simulations.

height $y_0$ + 1 mm or diffusion at height $y_0$ + 5 mm and $y_0$ + 10 mm. The differences between the two simulations come from the tabulated values for radicals in HTTC that are taken from premixed flamelets, which are slightly different from what is observed in FTC. Thus, some small discrepancies appear in the physical space as shown in Fig. 8 for $C_2H_5$ species. Despite these imperfections, the mass fraction field of major species the temperature and the propagation velocity of the flame tip are well reproduced by HTTC. With HTTC, the chemical time step is still larger than the convective time step, and simulations are performed approximately 5 times faster than with FTC. Actually, simulations with HTTC were first realized before switching to FTC ones in order to speedup the flame establishment and convergence.

Even though the HTTC simulations lead to satisfactory results by making use of tables based on 1D premixed flamelets, an even better agreement could be reached if diffusion effects were included in S2FT tables.

## 5. Conclusion

A $CH_4$/air edge flame with a strong mixture fraction gradient is simulated with three solvers featuring different models for detailed chemistry. The fully transported chemistry (FTC) is the reference case for the tabulated complex thermochemistry (CTC) and the hybrid chemistry (HTTC) approaches. Conventional techniques such as CTC modeling fail to predict such complex flame topology because only the structure of premixed

flamelets are tabulated without strain-rate-induced effects. However, it has been shown that the HTTC solver is capable of better capturing the shape, the propagation speed and the height of flame stabilization, even if the tabulated profiles are extracted from laminar premixed flames. With HTTC, the time-step is increased compared with detailed chemistry, and reaches values usually encountered for non-reactive flows with compressible solvers. Thus, the edge flame configuration is simulated with a computational cost divided by about 5. Future works should focus on the table generation procedure that could integrate constrained chemical equilibrium, on a direct comparison with a reduced chemistry on a challenging case and finally on the application of HTTC in the framework of Large-Eddy Simulation.

## Acknowledgments

Bastien Duboc was financially supported by the Region Haute-Normandie. Computations were performed using HPC resources from CRIANN. The preprocessing code to build up the HTTC table is available upon request at `https://www.coria-cfd.fr/index.php/HTTC`.

## References

[1] T. Lu, C. Law. *Prog. Energy Combust. Sci.*, 35:192–215, 2009.
[2] S.B. Pope. *Proc. Combust. Inst.*, 34:1–31, 2013.
[3] N. Jaouen, L. Vervisch, P. Domingo, G. Ribert. *Combust. Flame*, 175:60–79, 2017.
[4] O. Gicquel, N. Darabiha, D. Thevenin. *Proc. Combust. Inst.*, 28:1901–1908, 2000.
[5] J.A. van Oijen, F.A. Lammers, L.P.H. de Goey. *Combust. Sci. Tech.*, 127:2124–2134, 2001.
[6] G. Ribert, O. Gicquel, N. Darabiha, D. Veynante. *Combust. Flame*, 146(4):649–664, 2006.
[7] K. Wang, G. Ribert, P. Domingo, L. Vervisch. *Combust. Theory Model.*, 14:541–570, 2010.
[8] G. Ribert, K. Wang, L. Vervisch. *Fuel*, 91:87–92, 2012.
[9] P. Kourdis, J. Bellan. *Combust. Flame*, 161:1196–1223, 2014.
[10] G. Ribert, L. Vervisch, P. Domingo, Y.-S. Niu. *Flow, Turbul. Combust.*, 92:175–200, 2014.
[11] S. H. Chung. *Proc. Combust. Inst.*, 31(1):877–892, 2007.
[12] J. Hirschfelder, C. Curtiss, R. Byrd. *Molecular Theory of Gases and Liquids*. Wiley, New York, 1969.
[13] R. Vicquelin, B. Fiorina, S. Payet, N. Darabiha, Gicquel O. *Proc. Combust. Inst.*, 33(1):1481–1488, 2011.
[14] X. Petit, G. Ribert, P. Domingo. *J. Supercritical Fluids*, 101:1–16, 2015.
[15] P. Domingo, L. Vervisch, D. Veynante. *Combust. Flame*, 152:415–432, 2008.
[16] R. W. Bilger, S. H. Stårner, R. J. Kee. *Combust. Flame*, 80(2):135–149, 1990.
[17] G. Ribert, N. Zong, V. Yang, L. Pons, N. Darabiha, S. Candel. *Combust. Flame*, 154:319–330, 2008.
[18] L. Pons, N. Darabiha, S. Candel, G. Ribert, V. Yang. *Combust. Theory Model.*, 13:57–81, 2009.
[19] X. Petit, G. Ribert, G. Lartigue, P. Domingo. *J. Supercritical Fluids*, 84:61–73, 2013.
[20] L. Bouheraoua, P. Domingo, G. Ribert. *Combust. Flame*, 179:199–218, 2017.
[21] P. Lindstedt. *Proc. Combust. Inst.*, 27:269–285, 1998.
[22] C. D. Pierce, P. Moin. *J. Fluid Mech.*, 504:73–97, 2004.
[23] M. Ihme, C. M. Cha, H. Pitsch. *Proc. Combust. Inst.*, 30(1):793–800, 2005.
[24] G. Godel, P. Domingo, L. Vervisch. *Proc. Combust. Inst.*, 32(1):1555–1561, 2009.
[25] M. K. Kim, S. H. Won, S. H. Chung. *Proc. Combust. Inst.*, 31(1):901–908, 2007.
[26] A. M. Briones, S. K. Aggarwal, V. R. Katta. *Combust. Flame*, 153(3):367–383, 2008.
[27] P.-D. Nguyen, L. Vervisch, V. Subramanian, P. Domingo. *Combust. Flame*, 157(1):43–61, 2010.